Identification of Colon Cancer using Deep Learning Techniques

[1]Kantubhuktha Bhargavi, [2]Ravva Gurunadha
[1]*PG Scholar, Dept of Electronics and Communication Engineering (System and Signal Processing), University college of Engineering, JNTUK, Vijayanagram.*
[2]*Associate Professor, Dept of Electronics and Communication Engineering (System and Signal Processing), JNTUK, Vijayanagram*

Abstract **- The primary difficulty in distinguishing Colon Cancer Digital Pathology Photos is to differentiate benign from malignant disease. Colorectal cancer develops in the colon or the rectum. . Depending on where they originate, these cancers may be called colon cancer or rectal cancer, too. Since they have several characteristics in common, colon cancer and rectal cancer are frequently grouped together. Much of the current system relies on the characteristics of multiple frameworks that follow deep convolution neural networks (CNNs) used in the application of polyp detection in the current system, explaining the use of a deep learning model for polyp detection, while their system only achieved less than ideal accuracy (86%) and sensitivity (73%) and other methods. A standard support vector machine (SVM) classifier was trained to carry out polyp detection and classification of CNN features from a non-medical to a medical domain. Multi-scale fusion convolution neural network (MFF-CNN) feature based on shearlet transformation to classify histopathological picture of colon cancer Here we introduce the shearlet transformation approach fusion features and use VGG19 model that can provide better segmentation and classification accuracy for benign from malignant.**

Index Terms **- CNN, MF-CNN, Colon Cancer, VGG19, Shearlet Transformation.**

1.INTRODUCTION

Colorectal carcinoma (CRC) is one of the most difficult cancers to treat, as well as one of the leading causes of cancer-related death worldwide. According to contemporary epidemiological statistics, this type of cancer has a considerable burden in most European countries, and it is still associated with very high death rates (Mar- ley and Nan, 2016). As a result, for the life and well-being of a large number of patients, early tumour detection and distinction are crucial. Traditionally, pathologists diagnose CRC by visually inspecting resected tissue samples that have been preserved and stained with Hematoxylin and Eosin under a microscope (H&E). The presence and extent of malignancy are determined by observing the or- ganisational alterations in the tissues, which are highlighted by the two stains. Figure 1 depicts the organisation of typical colon tissues, with epithelial cells forming glandular structures and non-epithelial cells (stroma) lying in between. Adenoma is characterised by enlarged, hyperchromatic, and elongated nuclei structured in a layered manner, and is the most prevalent benign precursor to CRC. When compared to normal tissues, the adenoma appears tubular or villus. According to the literature, manual inspection has two major drawbacks. To begin with, it

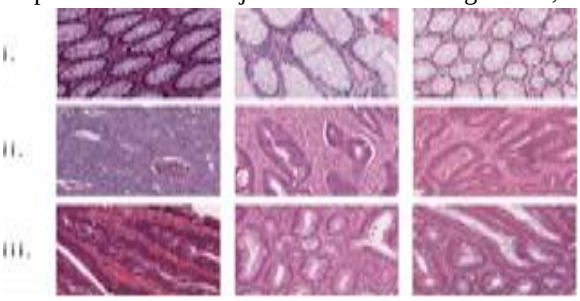

Fig 1 H&E photos of colorectal tissues histologically (cropped patches). Healthy tissue, adenocarcinoma, and tubulovillous adenoma are the three types of cancer.

Variability between and within observers (A. Young and Kerr, 2011). As a result, there are two key directions in which computer-aided diagnostic tools are being developed: I Automated segmentation to divide heterogeneous colorectal samples into homogenous (i.e., just one type of tissue) inter- est regions. (ii) automatic classification, which aims to

classify homogeneous tissue regions into one of several categories, such as normal or malignant, based on quantitative features extracted from the image. The high intra-class and inter-dataset variability that is inherent in histological imaging is the primary challenge to be overcome in both tasks. In this study, we focus on the automated classification challenge, specifically three histological criteria that are most important for CRC diagnosis: The three forms of tumours include healthy tissue, adenocarcinoma, and tubulovillous adenoma. In recent years, research on automated histological image categorization has developed, with applications encompassing anatomical areas other than the colon, such as the brain, breast, prostate, and lungs. The majority of the methods proposed involve automated texture analysis, which generates a small number of local descriptors from patches of the original input images and then feeds them into a classifier. Statistical characteristics such as the grey level co-occurrence matrix (GLCM), local binary patterns (LBP), Gabor and wavelet transforms, and others are often used. Texture descriptors are used by machine learning algorithms such as Support Vector Machines (SVM), Random Forests, and Logistic Regression classifiers, which are then encoded into a compact vocabulary of visual words (Di Cataldo and Fi- carra, 2017). Traditional texture analysis algorithms' endurance is severely constrained by their reliance on a set collection of handcrafted features, notwithstanding the great degree of accuracy attained by some of these studies. To begin with, it takes a thorough understanding of the visual traits that are best suited for classification, which is not always obvious. Second, it substantially limits the generalisation and transfer capabilities of the recommended classifiers, particularly in the face of inter-dataset variability.

2 LITERATURE SURVEY

Humans can only see a small portion of the electromagnetic spectrum. Different objects and materials generate light with their own electromagnetic signature, and since the 1960s, sensors have been employed to collect data on both visible and invisible regions of the spectrum to better capture these fingerprints.

Sensors that look at numerous narrow bands of the electromagnetic spectrum are used in hyperspectral imaging [8]. This enables the sensor to detect small alterations that would otherwise go undetected by typical imaging methods. These bands can cover the ultraviolet, visible, near-infrared, and short-wave infrared regions of the spectrum and range in size from 2 to 10 nm each. These images are spectrally and spatially smooth (neighbouring pixels and bands are substantially linked) [4. Using the colon cancer imaging data discussed in Chapter 4, a visual representation of these bands, called a hypercube, is illustrated in Fig. 3. A hyperspectral imager's light is frequently made up of a collection of constituent spectra known as endmembers. A combination of atmospheric factors, imager spatial resolution, and the existence of gaseous mixtures in the media blend these spectra together [4]. The endmembers in the figure [9] depict the pure materials. The materials that are deemed pure in a picture can differ depending on the subject being investigated. Materials that are highly reflective can also alter.

Hyperspectral imaging has expanded beyond remote sensing satellites thanks to technological advancements. Unmanned aerial vehicle (UAV) and ground-based commercial and research options incorporating hyperspectral imaging have been expanded thanks to smaller camera sizes and more efficient storage. One of the potential applications of hyperspectral imaging is precision agriculture. Farmers can utilise hyperspectral photos to better monitor their crops if they have access to UAVs. Disease, water stress levels, crop nutrients, invasive insects, nutritional deficits, and soil toxins can all be detected using hyperspectral pictures. This allows farmers to detect problems long before they manifest themselves visually [8]. Another potential application of hyperspectral imaging is fresh water resource management. Hyperspectral imaging can be used to offer precise estimations of available ground water as well as flood early warning and monitoring. It can also provide details on the water quality available. Hyperspectral imaging can detect any biological or biochemical pollutant, as well as quantify chemical oxygen and chlorophyll concentration in water [8].

There are numerous defence and homeland security applications for hyperspectral imaging. Methods for detecting hyperspectral anomalies can quickly distinguish between targets and the background. On the ground, a combination of classification algorithms such as support vector machines and linear unmixing

can be employed to use hyperspectral imagery as a tool for facial identification [8]. It can also be used to detect face stress by measuring changes in a subject's blood oxygen levels.

Hyperspectral imaging is also being used more on the ground in food safety and quality applications. These images are great for monitoring food quality and detecting spoilage and pollutants since they contain a wealth of spatial and spectral information. The hardness of blueberries and the fat content of pork chops have both been assessed using hyperspectral imaging [8]. Hyperspectral imaging can also be used in art and forensics. Spectral signatures can aid in the detection of forgeries and the authentication of the worth of particular items [8]. Many medical diagnostic applications for hyperspectral imaging exist, including bruising and burn diagnosis, cancer screening, and surgery aid [10]. Hyperspectral imaging has also been demonstrated to be effective in the detection of haemorrhage, diabetes, and other cancers. It's being investigated as a possible replacement for computed tomography and magnetic resonance imaging [8].

3 PROBLEM DEFINITION

Imaging and machine literacy have been investigated in cancer research and treatment for a variety of cancers, including bone, liver, colon, bladder, and pancreatic cancer. Support vector machines and arbitrary support vector machines are the most used machine literacy tools for cancer discovery. Bayesian networks, timbers K-nearest neighbour algorithms and arbitrary timbers are examples of colon cancer finding styles. Despite the fact that traditional machine learning algorithms play an important role in the automatic detection of colorectal cancer, they still fall short of an expert endoscopist's judgement. Only a few studies in the field of colorectal cancer diagnosis have used deep learning.

4 PROPOSED APPROACH

To categorise the histological picture of colon cancer, researchers used a multi-scale fusion convolution neural network (MFF-CNN) feature based on shearlet transformation. Here, we introduce the shearlet transformation approach, fusion features, and VGG16 architecture, which can improve benign from malignant segmentation and classification accuracy.

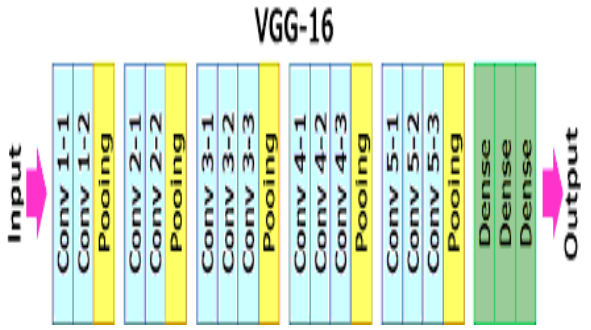

Fig 2:-vgg model

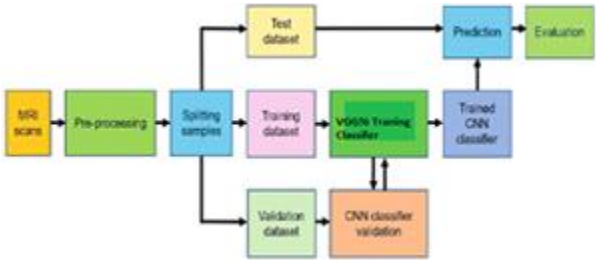

Fig 3:-Block diagram colon caner prediction

4.1 Methdology

4.1.1 DataSet

The dataset was collected from the below link

- https://academictorrents.com/details/7a638ed187a6180fd6e464b3666a6ea0499af4af
- 1.8 gb data set of CT_Scan images are avaible in this link

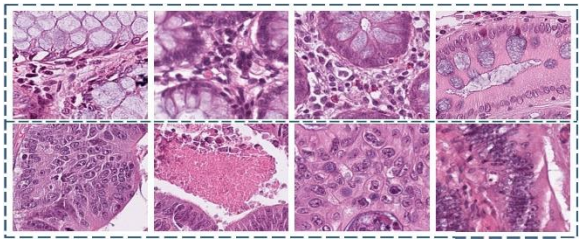

Fig 5:- Image patches of normal colon mucosa (negative class) are on the top row, whereas image patches of colorectal cancer epithelium (positive class) are on the bottom row.

4.1.2 PREPROCESSING:

After selecting the most relevant input data, the neural network must be pre-processed to ensure that the neural network produces accurate results. This decreases the quantity of inputs to the network, making it easier for it to learn. It eliminates undesired signals from CT scans. Color photos are converted to grey-level coding.

4.1 3 MFF-CNN

The MFF CNN classifier's performance was assessed in terms of training and classification accuracy. This network is a type of radial basis network that provides fast and accurate classification and is a promising technique for defect classification from good material. Existing weights will never be changed; instead, during training, new vectors will be added into weight matrices. As a result, it is possible to use it in real-time. MFF CNN is particularly quick since the training and execution procedures may be implemented using matrix manipulation.

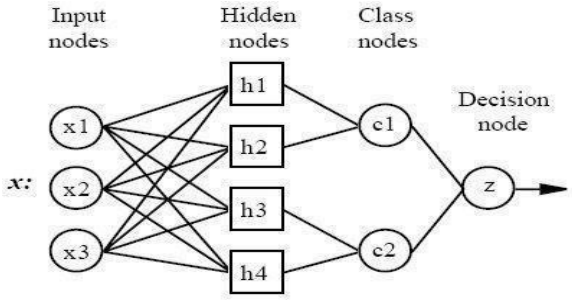

Fig 4- Architecture of MFF_CNN

4.1 4 Layers

In classification challenges, LAYERS MFF CNN is frequently employed. The first layer calculates the distance between the input vector and the training input vectors when an input is present. This generates a vector whose members represent how similar the input is to the training input. The second layer adds up each input's contribution and produces a net output as a vector of probabilities. Finally, a full transfer function on the second layer's output selects the highest of these probabilities, producing a 1 (positive identification) for that class and a 0 (negative identification) for non-targeted classes.

4.1 5 INPUT LAYER

Each predictor variable is represented by a neuron in the input layer. When there are N categories in a categorical variable, N-1 neurons are used. By subtracting the median and dividing by the inter quartile range, the range of data is standardized. The values are then fed to each of the neurons in the hidden layer by the input neurons.

4.1.5. 1 LAYER OF THE PATTERN

Each case in the training data set has one neuron in this layer. It saves the values of the case's predictor variables as well as the target value. A hidden neuron calculates the Euclidean distance between the test case and the neuron's center point, then uses the sigma values to apply the radial basis function kernel function.

4.1.5. 2 LAYERS OF SUMMATION

Each category of the target variable has one pattern neuron in MFF CNN networks. Each hidden neuron stores the actual target category of each training event; the weighted value output by a hidden neuron is only supplied to the pattern neuron that corresponds to the hidden neuron's category. The values for the class that the pattern neurons represent are added together.

5 ALGORITHMS USED

To build a deep learning network for abnormalities detection using CNN we propose a structure with three convolutional layers as follows:

- step 1: 16 Convolutions layer with filter mask of size 3x3x1 and padding filter [1111].
- Step2: Maxpooling layer with filter mask size 2x2 max pooling with stride [2 2] and padding filter [0000].
- Step 3: Activate layer
- step 4: 32 Convolutions layer with filter mask of size 3x3x16 and padding filter [1111].
- Step5: Maxpooling layer with filter mask size 2x2 max pooling with stride [2 2] and padding filter [0000].
- Step 6: Activate layer
- step 7: 240 Convolutions layer with filter mask of size 3x3x32 and padding filter [1111].

Fig 6:-MFCNN algorithm steps

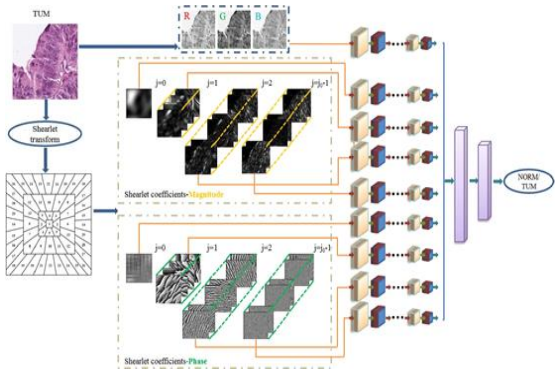

Fig 7: Module Implementation

6 RESULTS AND EVOLUTION METRICS

Fig 8:- masked image from sample input image

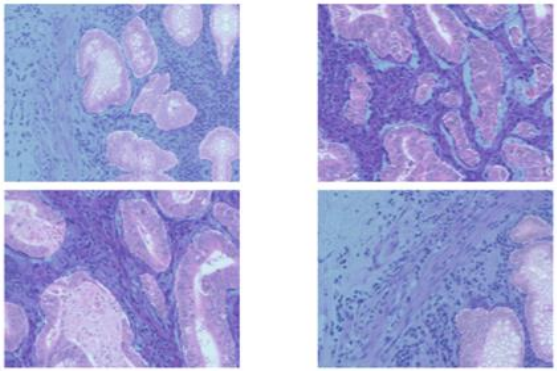

Fig 9:- masked images from batch data

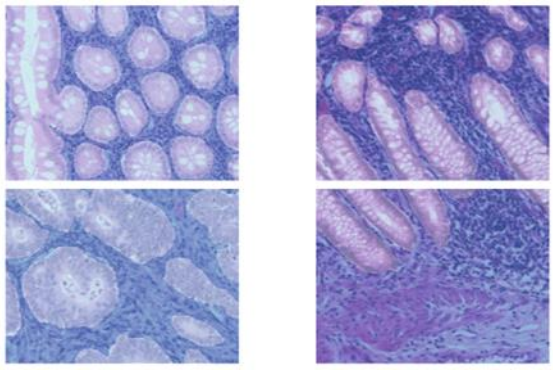

Fig 10 Segmented image of batch data

epoch	train_loss	valid_loss	my_dice	my_acc	time
0	2.592335	1.313381	0.095876	0.501146	00:23
1	1.561479	0.819113	0.648587	0.554937	00:23
2	1.151163	0.622113	0.652725	0.684121	00:23
3	0.909205	0.466463	0.752626	0.790209	00:23
4	0.741706	0.456414	0.771634	0.793708	00:23
5	0.658178	0.618646	0.528618	0.672664	00:23
6	0.599220	0.437910	0.817843	0.820894	00:23
7	0.515297	0.368805	0.822246	0.844712	00:23
8	0.518789	0.349211	0.825800	0.848334	00:23
9	0.507438	0.559643	0.778084	0.758841	00:23
10	0.468400	0.376684	0.803178	0.836248	00:23
11	0.422757	0.323809	0.853187	0.862358	00:23
12	0.394347	0.418876	0.782699	0.823149	00:23
13	0.400295	0.349912	0.845961	0.851626	00:23
14	0.375370	0.296458	0.853277	0.873472	00:23
15	0.355698	0.288872	0.869037	0.880706	00:23
16	0.325250	0.289112	0.865725	0.876428	00:23
17	0.331336	0.445767	0.808181	0.815013	00:23
18	0.340328	0.261187	0.879618	0.892455	00:23
19	0.310067	0.294144	0.872315	0.883448	00:23
20	0.294486	0.307285	0.868957	0.882012	00:23
21	0.282775	0.341456	0.827894	0.858952	00:23
22	0.276114	0.295241	0.873748	0.882959	00:23
23	0.259618	0.293406	0.872939	0.887532	00:23

Fig11: _ Accuracy at 23 epochs is 88.73%

25	0.231586	0.276360	0.879713	0.889266	00:23
26	0.217991	0.256066	0.887826	0.896135	00:23
27	0.209909	0.293946	0.862079	0.890065	00:23
28	0.209163	0.291820	0.870664	0.878483	00:23
29	0.205368	0.285454	0.881198	0.888052	00:23
30	0.192430	0.271557	0.891225	0.898088	00:23
31	0.186877	0.241008	0.891762	0.902465	00:23
32	0.179201	0.265498	0.890055	0.897603	00:23
33	0.171099	0.290673	0.890193	0.896448	00:23
34	0.168599	0.410401	0.881596	0.883561	00:23
35	0.167345	0.277747	0.882109	0.887613	00:23
36	0.161932	0.226558	0.906133	0.913466	00:23
37	0.159961	0.276201	0.893306	0.904401	00:23
38	0.158659	0.241091	0.900951	0.910082	00:23
39	0.153294	0.239724	0.901761	0.909761	00:23
40	0.145207	0.256236	0.898413	0.906042	00:23
41	0.138018	0.255820	0.901656	0.909601	00:23
42	0.130477	0.256706	0.900792	0.909232	00:23
43	0.130194	0.262502	0.900285	0.908392	00:23
44	0.127596	0.257114	0.900542	0.908092	00:23
45	0.125775	0.263379	0.900876	0.908405	00:23
46	0.127104	0.260280	0.900377	0.908332	00:23
47	0.123434	0.253082	0.902603	0.910245	00:23
48	0.120448	0.254120	0.901976	0.909656	00:23
49	0.121144	0.254726	0.901901	0.909289	00:23

Fig12:_ Accuracy at 50 epochs is 90.92%

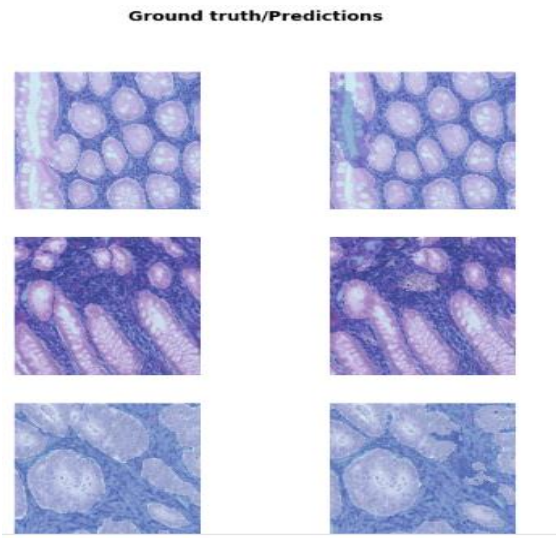

Fig13:_ Ground truth and predicted images

31	0.095962	0.251991	0.911428	0.919612	00:23
32	0.094233	0.246141	0.909259	0.917440	00:24
33	0.091785	0.246146	0.911764	0.920033	00:23
34	0.090846	0.255872	0.908357	0.917989	00:23
35	0.090526	0.239993	0.912862	0.922481	00:23
36	0.088635	0.244325	0.912086	0.922237	00:23
37	0.088234	0.243842	0.912755	0.921348	00:23
38	0.086883	0.241405	0.913024	0.922980	00:24
39	0.085949	0.242298	0.911951	0.921067	00:23
40	0.086274	0.232635	0.913331	0.922387	00:23
41	0.085257	0.245231	0.912673	0.921436	00:23
42	0.083929	0.254990	0.911373	0.920517	00:24
43	0.083822	0.243979	0.913105	0.921639	00:23
44	0.082324	0.237289	0.914132	0.922962	00:23
45	0.082796	0.244143	0.912590	0.921760	00:23
46	0.083741	0.242331	0.914185	0.922843	00:23
47	0.084133	0.244931	0.912597	0.921379	00:23
48	0.082498	0.243090	0.912715	0.921612	00:23
49	0.083154	0.234266	0.914594	0.923685	00:23

Fig14:_ Accuracy at stage 2 92.36% at 50 epochs

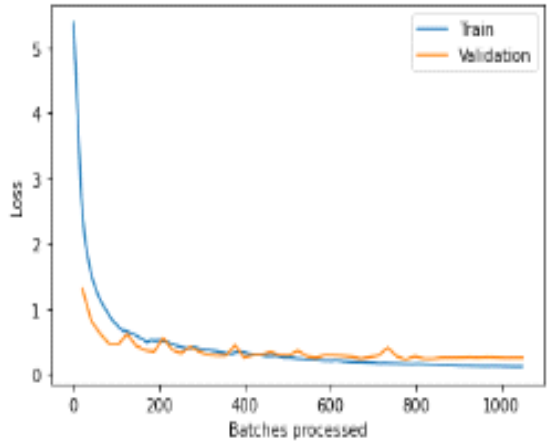

Fig 15: -training and validation loss graph with different batch size Validation loss graph at stage 2

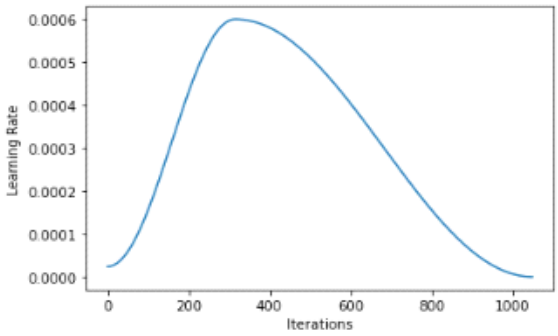

Fig 16: -learning rate graph at 50 epochs 0.0005

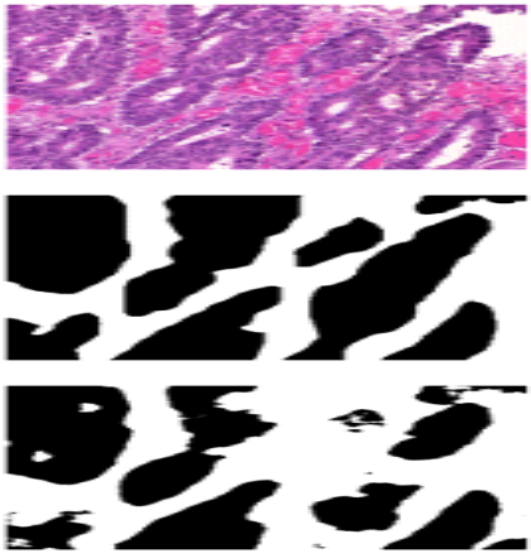

Fig 17: -Segmented Image after 50 ephcos

7 CONCLUSION

The medical therapy of colon cancer necessitates real-time, objective, and precise diagnosis. Existing identification approaches rely on hand-crafted feature extraction, which takes a long time to complete and excludes the optimal treatment option. For categorising colon lesions autonomously, the study offers an MFF-CNN architecture based on the shearlet transform. We have four proposals for comparing the contributions of the magnitude and phase coefficients in order to increase classification accuracy. These suggestions are possible coefficient combinations and are supplied as supplementary information. The data suggested that the MFF-CNN might increase performance significantly.

REFERENCES

[1] Young, R. H. and Kerr, D. (2011). *ABC of Colorectal Cancer*. Wiley-Blackwell, 2nd edition.

[2] Chollet, F. et al. (2015).Keras. https://github.com /fchollet/keras.

[3] Di Cataldo, S. and Ficarra, E. (2017). Mining textu- ral knowledge in biological images: Applications, methods and trends. *Computational and Structural Biotechnology Journal*, 15:56 – 67.

[4] Hastie, T., Tibshirani, R., and Friedman, J. (2009). Overview of supervised learning. In *The elements of statistical learning*. Springer.

[5] Janowczyk, A. and Madabhushi, A. (2016). Deep learn- ing for digital pathology image analysis: A compre- hensive tutorial with selected use cases. *Journal of Pathology Informatics*, 7(1):29.

[6] Korbar, B., Olofson, A. M., Miraflor, A. P., Nicka, C. M., Suriawinata, M. A., Torresani, L., Suriawinata, A. A., and Hassanpour, S. (2017). Deep learning for clas- sification of colorectal polyps on whole-slide images. *Journal of Pathology Informatics*, 8:30.

[7] Maaten, L. v. d. and Hinton, G. (2008). Visualizing data using t-sne. *Journal of Machine Learning Research*, 9(Nov):2579–2605.

[8] Marley, A. R. and Nan, H. (2016). Epidemiology of col- orectal cancer. *International Journal of Molecular Epidemiology and Genetics*, 7(3):105–114.

[9] Qian, N. (1999). On the momentum term in gradi- ent descent learning algorithms. *Neural networks*, 12(1):145–151.

[10] Simonyan, K. and Zisserman, A. (2014). Very deep con- volutional networks for large-scale image recognition. *arXiv preprint arXiv:1409.1556*.

[11] Weiss, K., Khoshgoftaar, T. M., and Wang, D. (2016). A survey of transfer learning. *Journal of Big Data*, 3(1):9.

[12] Yao, Y., Rosasco, L., and Caponnetto, A. (2007). On early stopping in gradient descent learning. *Constructive Approximation*, 26(2):289–315.

[13] Xu, Y., Li, Y., Liu, M., Wang, Y., Lai, M., Eric, I. and Chang, C., 2016, October. Gland instance segmentation by deep multichannel side supervision. In *International Conference on Medical Image Computing and Computer-Assisted Intervention* (pp. 496-504). Springer, Cham.

[14] Yang, L., Zhang, Y., Chen, J., Zhang, S. and Chen, D.Z., 2017, September. Suggestive annotation: A deep active learning framework for biomedical image segmentation. In *International Conference on Medical Image Computing and Computer-Assisted Intervention* (pp. 399-407). Springer, Cham.

[15] Yang, W., Guo, L., Zhao, T. and Xiao, G., 2007, May. Improving watersheds image segmentation method with graph theory. In *Industrial Electronics and Applications, 2007. ICIEA 2007. 2nd IEEE Conference on* (pp. 2550-2553). IEEE.

[16] Yuheng, S. and Hao, Y., 2017. Image Segmentation Algorithms Overview. *arXiv preprint arXiv:1707.02051*.ahn, C.T., 1970. Graph theoretical methods for detecting and describing gestalt clusters.

[17] *IEEE Trans. Comput.*, *20*(SLAC-PUB-0672-REV), p.68. Zhang, Y., Matuszewski, B.J., Shark, L.K. and Moore, C.J., 2008, July. Medical image segmentation using new hybrid level-set method. In *Fifth International Conference BioMedical Visualization: Information Visualization in Medical and Biomedical Informatics* (pp. 71-76). IEEE.

[18] Zhao, G., Ahonen, T., Matas, J. and Pietikainen, M., 2012. Rotation-invariant image and video description with local binary pattern features. IEEE Transactions on Image Processing, 21(4), pp.1465-1477.

[19] Zhu, R., Sang, G., Cai, Y., You, J. and Zhao, Q., 2013. Head pose estimation with improved random regression forests. In *Biometric Recognition* (pp. 457-465). Springer, Heidelberg.